ANL/MSD/CP-95845

58930-00-105
58712-00-105

Refracted X-ray Fluorescence (RXF) Applied to the Study of Thermally Grown Oxide Scales on Fe-Cr-Ni-(RE) Alloys

I. Koshelev, A.P. Paulikas, and B.W. Veal

Materials Science Division
Argonne National Laboratory, Argonne, IL 60439

Proceedings of 193rd Meeting of the Electrochemical Society, San Diego, CA, May 3-8, 1998

This work supported by the U.S. Department of Energy, Basic Energy Sciences-Material Sciences under contract #W-31-109-ENG-38.

DISCLAIMER

REFRACTED X-RAY FLUORESCENCE (RXF) APPLIED TO THE STUDY OF THERMALLY GROWN OXIDE SCALES ON FE-CR-NI-(RE) ALLOYS

I. Koshelev, A.P. Paulikas, and B. W. Veal,
Argonne National Laboratory , Argonne, Ill 60439

Refracted X-Ray Fluorescence (RXF) is applied to the study of the thermally grown scales on Fe25Cr20Ni(RE) alloys. The evolution of chromia scales is investigated for alloys containing reactive elements (RE) Y and Zr as well as the corresponding RE-free alloy. For these alloys, scale compositions, scale thicknesses and growth rates are measured and information about concentration depth profiles is obtained.

INTRODUCTION

Grazing-emission RXF has been applied to the investigation of ultra thin films on semiconductors (1), analysis of ion implantation profiles (2) and thin film deposition (3). A near-grazing-angle x-ray fluorescence technique, RXF is suited for the investigation of surfaces and interfaces of solids at high temperature and in otherwise hostile environments, and allows determination of compositions, composition profiles, scale thicknesses and growth rates. In this paper results of an investigation of the early stages of oxidation of austenitic Fe-CR-Ni steels with Y and Zr reactive elements are presented.

The primary experimental technique used in this study was refractive X-Ray fluorescence (RXF). It was used to obtain nondestructive concentration depth profiles of various elements found in the oxide scales as the scales formed (i.e.., during the oxidation process). The RXF technique measures the integrated intensity of x-ray fluorescence, emitted from a flat sample surface into a fixed acceptance window (detector), as a function of fluorescence emission angle. The pickoff angle is normally scanned at angles close to grazing emission. Generally the scan passes through the critical angle for total external reflection, where the emission intensity changes abruptly and surface sensitivity varies rapidly. When the pickoff angle of the detector is varied, the escape depth of x-rays from the material, and hence the probe depth available for analysis, correspondingly varies. At pickoff angles less than the critical angle for total external reflection, the escape depth for x-rays is extremely small, usually tens to hundreds of Angstroms. The critical angle depends on the electron density in the sample and the wavelength of the fluorescent radiation. Typical values of critical angle fall in the range of several to tens of milliradians. At angles much larger than critical, escape depths are proportional to the sine of the emission angle. Escape depth also depend on sample composition and energy of the emitted x-rays through a linear absorption coefficient. For 3d transition elements (e.g., Cr through Ni) the maximum probe depth can be as large as tens of microns.

The total measured fluorescence intensity, detected on the vacuum side of the interface at angle α_v with respect to the surface, which is emitted from an element present in concentration $C(z)$ inside the solid, is

$$I(\alpha_v) = Const \int_{\alpha_v-\Delta}^{\alpha_v+\Delta} \int_z C(z) Inst(\alpha_v, \alpha_v') I(z, \alpha_v') \exp(-\mu_i z / \sin\alpha_i) dz d\alpha_v' \qquad [1]$$

where z is distance (depth) from the surface and *Const* includes factors such as the illuminating intensity, the probability of ionization of an atom of the emitting element by the illuminating radiation, the probability for emission of an x-ray of the detected energy from this excited atom, and the response of the detector. We assume illumination by a monoenergetic beam of x-rays whose energy is above the absorption edge of the element of interest. $Inst(\alpha_V, \alpha_V')$ is the aperture function of the detector which has an acceptance half-angle Δ of about one milliradian. μ_I is the linear absorption coefficient for the illuminating x-rays; α_i is the angle at which the illuminating radiation enters the sample, fixed at about ten degrees in our experiment. $I(z, \alpha_V)$ is the intensity from a point source of radiation, inside the semi-infinite medium, at the distance z below the surface, which reaches the detector positioned at the angle α_V. Eq. [1] must deal with any absorption, reflection, or refraction at any interface that might be encountered on the path between source and detector. If there are multiple film layers, contributions from all layers and the substrate must be properly considered (4). There are a number of approaches for treating this problem (4,5); our approach has been developed in detail in (6). Possible effects attributable to secondary emission in the samples were not considered; any effect dealing with secondary fluorescence are implicitly incorporated into the terms *Const* and μ_i.

Because oxides usually have an electronic density lower than that of the base metal, they have smaller critical angles. Thus, for oxidized material, emission from the scale usually appears as additional structure at low angles. Various transition metal oxides often produce very similar "fingerprints" in the RXF spectra since they have relatively comparable electronic density and absorption properties. For example, critical angles for different iron oxides and spinels are very similar (Table 1); detection of critical angle differences of less than one milliradian is required for their identification.

The RXF technique is element selective. It allows for simultaneously investigating the angle dependence of the spectra emitted by all the elements in the sample.

EXPERIMENTAL

In this paper we report studies of the oxidation of the Fe25Cr20Ni, Fe25Cr20Ni3Zr and Fe25Cr20Ni0.3Y where compositions are specified in weight %. The samples were prepared from high purity materials in an arc furnace in a He/Ar atmosphere and were rolled into sheets of approximately 1 mm thickness. Samples were cut into 1.5 x 2 cm^2 plates and were polished with 0.1 micron diamond paste before the oxidation treatments.

Oxidation was performed in an experimental chamber designed for studying fluorescence spectra at emission angles near grazing in controlled environments (7). The base pressure in the chamber was $\approx 10^{-4}$ Pa. The illuminating (exciting) radiation was provided by a Cr anode x-ray tube which was operated at 25 kV and 40 ma. A Si(Li) x-ray

detector was used. Samples were illuminated at a fixed angle of ~10 degrees. The angular dependence of the intensity of fluorescent radiation was measured from 0 to 80 milliradians relative to the sample surface. The angular resolution of the accepted radiation was ~2 milliradians.

Oxidation was carried out using two different procedures. In one procedure, samples were oxidized at a fixed temperature for 1 hr in 13.3 Pa of oxygen, then measurements were taken at room temperature in a vacuum $\approx 10^{-4}$ Pa. The first oxidation step was done at 450 °C. Sequential oxidations were done in 50 °C increments to 800 °C. Systematic variations in $I(\alpha)$, caused by different degrees of oxidation, of the accessible fluorescence lines (the $K\alpha$ and $K\beta$ lines of Cr, Fe, and Ni) were measured.

The second procedure was an isothermal oxidation, which was performed at 700 °C for 25 hr. The intensity of fluorescent radiation from the sample was measured at the elevated temperature during oxidation at a pressure of 13.3 Pa. A Laue diffraction line from a sapphire standard fixed to the specimen was observed, superimposed on the fluorescence $I(\alpha)$ scan. In both procedures, to obtain reproducible detector angle positions relative to grazing, $I(\alpha)$ spectra were compared after bringing the Laue line into coincidence. With this technique, the detector position could be reproduced with better than 1 milliradian precision.

In the experimental geometry, Cr $K\alpha$ fluorescence from the sample was by chance superimposed on a Bragg diffraction peak attributable to Cr $K\alpha$ characteristic radiation (from the x-ray tube) diffracting from the fcc lattice of the polycrystalline Fe-Cr-Ni sample. Presence of the diffraction peak complicated analysis of Cr $K\alpha$ refracted fluorescence radiation from the samples. Consequently, for Cr emission, only an analysis of Cr $K\beta$ fluorescence is presented.

Additional information about oxidation behavior of the samples was obtained after the final stage of oxidation. Scanning electron microscopy (secondary emission and EDX) was performed on a Hitachi S-2700 in order to view the morphology of the developed oxide scales, to measure the cross-sections of the scales, and to measure the concentration of the elements in the scale.

Cyclic Oxidation of the Samples.

Early stage oxidation behavior of bulk samples of Fe25Cr20Ni, Fe25Cr20Ni0.3Y and Fe25Cr20Ni3Zr alloys was studied after oxidation and subsequent cooling to room temperature, i.e., in a thermal cycling mode. Raw data for the intensity of the Ni $K\alpha$ and Cr $K\beta$ fluorescent radiation from the samples are shown in Fig. 1. $I(\alpha)$ spectra are presented for several temperatures of oxidation. Fluorescence signals from both the oxide layer and from the underlying bulk contribute to the measured intensity. For the data in Fig. 1 fluorescent radiation at high emission angles comes predominantly from the metallic substrate and, at low emission angles, predominantly from the oxide. Because the oxide scales have larger indices of refraction (lower electronic densities) than the metal substrate,

they have smaller critical angles. Consequently, the leading edge structure at low take-off angles is enhanced with the appearance of an oxide scale. Calculated values of the critical angles α_c, escape depth at critical angles $D(\alpha_c)$, and escape depth at normal emission D(90°) are shown in Table 1 for the base alloy and for several oxides that are likely to appear in the scale,.

Although not striking, signatures of the expected transitional oxides are revealed to varying degrees in a close inspection of the leading edges of the $I(\alpha)$ spectra of all three alloys collected after the lowest (450 - 600 °C) temperature oxidations (not all shown). The Fe, Ni and Cr spectra develop tails at angles which are below the critical angle for the metal. There are differences between the signatures of the transient oxides of the three alloys, but systematic difficulties such as insufficient accuracy in the measurement of the emission angle α constrain further analysis of transitional oxide evolution at this time. At the higher oxidation temperatures, the behavior of Cr RXF is profoundly different from that of Fe or Ni (Fig 1). $I(\alpha)$ spectra for Cr increase systematically with oxidation (note the linear scale) while the intensities for Fe and Ni decline (note the logarithmic scales). This occurs because, as the scale matures, a dominantly chromia scale forms, increasing the Cr atom density at the surface while increasingly covering Fe and Ni atoms of the substrate. The growth of the chromia scale occurs through (and beyond) a range of thickness (tens through thousands of Angstroms) which has a characteristic signature in $I(\alpha)$ (6), a distinctively peaked structure near the critical angle. Analysis of the shape of the spectrum in this thickness range can be used to determine the thickness of the scale.

A reliable measurement of the thickness of the oxide scale is important as a foundation for further analysis. Because absorption lengths normally increase with increasing photon energy, the relative change in intensity for $K\beta$ lines traversing a sample of given thickness is smaller than the relative intensity change for $K\alpha$ lines of the same element. The measured intensity ratio of Fe $K\beta$ to Fe $K\alpha$ (or Ni $K\beta$ to Ni $K\alpha$) obtained at high emission angle will be a function of the absorption properties and thickness of the oxide scale only. Consequently, one can use this intensity ratio to determine the thickness of the overlying chromia scale (6). We have used this technique to measure the thicknesses of the chromia scale, developed during cycling oxidation, on FeCrNi, FeCrNiY and FeCrNiZr. The thicknesses of these scales are shown in Fig. 2. Although scale thicknesses apparently develop at different rates, the alloy with Y develops the thinnest scale after the final treatment (~9800 Å ±10%). The base alloy, without reactive element, develops the thickest scale (~12000 Å.). Thicknesses of the scales on these two alloys were also obtained from cross-section measurements after the sequence of oxidations was completed; they are ~0.8-0.9 microns for the Y-containing specimen, and ~1-1.2 microns for the base (RE free) alloy, in reasonable agreement with the fluorescence thickness measurements. If the composition and absorption properties of a film are known, the thickness of the film can also be determined by fitting of the theoretical model (Eq. [1]) to the distinctive $I(\alpha)$ spectrum described in the previous paragraph. Using the Cr $K\beta$ fluorescent radiation, thicknesses were determined at each stage of the oxidation of the samples. Results of this modeling are also in reasonable agreement with those calculated from Fe $K\alpha$/Fe $K\beta$ intensity ratios which are shown in Fig 2.

The chromium fluorescence from the growing chromia scale is the dominant radiation emanating from all three alloys as the scale matures. However, differences between the alloys in the details of the subduction of Fe and Ni are quite apparent. Simulation of the spectral functions $I(\alpha)$, using Eq.[1] as described in (6), for the Fe Kα and Ni Kα radiation (Fig. 1) shows that these spectral functions can not be described solely by absorption of the fluorescent radiation, originating in the substrate, by an overlying chromia scale (Fig. 3, lowest lines). This implies the presence of Fe and Ni in the predominantly chromia scale.

Assuming a given distribution of Fe and Ni in the dominantly chromia scale, one can calculate appropriate $I(\alpha)$ for each element and compare the model calculations with the measurements.. This is a procedure which requires self-consistency because the introduction of some Fe or Ni emitters into the (modeled) scale changes the scale's absorption properties for the Fe and Ni fluorescence radiation and consequently changes the intensity signature $I(\alpha)$ from the Fe and Ni in the scale. Moreover, while fluorescence from Ni atoms is free from secondary emission enhancement, intensity of the Fe Kα line is subject to secondary emission considerations. In our calculation it was assumed that the intensity from Fe atoms in the chromia scale experiences the same enhancement due to secondary emission as does the intensity coming from the Fe atoms in the alloy. We first consider a model in which the Fe and Ni are distributed uniformly, at a concentration to be determined by fit to the data, throughout the (previously determined) thickness of the chromia scale. Such a model yields the functional dependence on emission angle shown in Fig. 3. It is evident that such a model, while narrowing the range of conceivable minority element concentration in the scale, inadequately describes the data, i.e., at least one more parameter can be can be extracted from the data. We thus feel justified in increasing the complexity of the model. The additional adjustable parameter which we add to the model is a second thickness -- the thickness of the scale, measured from the scale-metal interface, in which Ni or Fe is present at a concentration which is, as previously, to be determined. An example of the correspondence between such a double layer model and the data is provided in Fig. 4. We confine ourselves at present to fitting the $I(\alpha)$ data for Fe and Ni fluorescence radiation to this double layer model. The parameters which were found to fit the double layer model are presented in Table II.

The results in Table II show that Ni and Fe atoms in the chromia scales of the alloy with Y do not, at the highest temperature studied, diffuse as far into the scale from the underlying alloy as they do in the alloy containing Zr or in the base alloy without reactive elements. We note that we have restricted ourselves to analyzing the relatively mature scale (700-800 °C) in the context of the two layer model; although evidence of the presence of the transient scale formed at temperatures below 700 °C is observable, limited accuracy of emission angle measurement restricts our ability to analyze the subtle changes that occur at the critical angle as the transient scale is forming. We also note that there is a qualitative difference in the Ni $I(\alpha)$ of the Y-containing alloy compared to the other two. The persistent bump at low emission angles is a distinct signature of the presence of a small amount of Ni right on the surface of the Fe25Cr20Ni0.3Y alloy; no such feature is seen in the Ni $I(\alpha)$ of the other two alloys. We can estimate that on the order of 200 Å of Ni, uniformly distributed on the surface of the 800 °C oxidized Fe25Cr20Ni0.3Y, would be consistent with this observation. We further note that there was no evidence of such a thin

stratum of Ni on the surface of the same alloy when it was subjected to a monotonically increasing temperature of oxidation (no thermal cycling) (6). The compositions of the scales, determined by EDX measurements of the cross section of the scales after the final (800 °C) oxidation, are shown in Table III.

In these measurements the diameter of the electron probe is approximately 1 micron; this is comparable to the thickness of the scales, thus concentrations of Fe and Ni may be distorted (overestimated) because of the contribution from the substrate.

Isothermal oxidation.

As was emphasized before, the measured intensity ratio of Fe $K\beta$ to Fe $K\alpha$ (or Ni $K\beta$ to Ni $K\alpha$) obtained at high emission angle allows one to calculate the thickness of the overlying chromia This is useful in measuring, in situ, the thickness of the scale as a function of time of oxidation provided that the composition of the scale is known. In the case of isothermal oxidation one thus obtains a measurement of the oxidation rate.

It was established in the previous cycling oxidation experiments that the chromia scale starts to dominate at 600 °C, while hematite, nickel oxide or spinels become minor constituents. Thus, expecting the major constituent of the scale to be chromia, measurements of isothermal oxidation were performed at 700 °C. During the oxidation, the intensities of the fluorescent x-rays of Ni, Fe and Cr (the $K\alpha$ and $K\beta$ lines of each element) were monitored at a fixed emission angle of 88 milliradians. The thickness of the overlying chromia scale was calculated from the relative attenuation of the Fe $K\beta$ to Fe $K\alpha$ lines. Results of the measurement of the thickness of the scales growing on the Fe25Cr20Ni, Fe25Cr20Ni0.3Y, and Fe25Cr20Ni3Zr alloys during the isothermal oxidation are shown in Fig. 5. After 25 hours of oxidation, scales thicknesses of 10000Å, 8600Å and 9300Å respectively were developed. These results are in the good agreement with the thicknesses which were obtained from cross-section measurements. Measurement of the cross-sections of the samples after isothermal oxidation (compositions shown in Table IV) yielded thickness of the scales of approximately 1, 0.8 and 0.9 microns for the Fe25Cr20Ni, Fe25Cr20Ni0.3Y, and Fe25Cr20Ni3Zr alloys. Good agreement is explained by: 1) good adhesion of the scales which grew during the isothermal oxidation, 2) absence of visible cracks and porosity, and 3) low concentration of Fe and Ni in the scales (EDX analysis of the cross-sections gave concentration of Fe and Ni in the scales 1/3 to 1/4 of the concentration of these elements found in the scales developed during cyclic oxidation).

The solid lines in Fig. 5 are parabolas. Assuming that the parabolic law of oxidation is valid for these alloys, we obtain the constants 1.23×10^{-13} cm^2/sec, 8.1×10^{-14} cm^2/sec and 1.02×10^{-13} cm^2/sec for the Fe25Cr20Ni, Fe25Cr20Ni0.3Y, and Fe25Cr20Ni3Zr alloys respectively. The oxidation constant is K in the parabolic equation of oxidation $d^2=Kpt$ (d is thickness and t is time). These relatively high oxidation rates can not be explained by the lattice and low-angle boundary diffusivities. It is commonly believed that the rate-controlling process is cation diffusion along high-angle grain boundaries (or another short circuit path)(8,9). In has been found in many studies that RE or RE oxide incorporation into the base alloy improves the oxidation properties by retarding

the growth rate of the chromia. This is the case in our system also -- the sample with Y as RE shows the lowest scale growth rate. However, the relative differences among the oxidation rates for these samples at 700 °C can not be considered large.

CONCLUSIONS

Evolution of the thermally grown oxide scales on the austenitic steels Fe25Cr20Ni, Fe25Cr20Ni0.3Y , Fe25Cr20Ni3Zr was studied by refracted x-ray fluorescence. The angle dependence of fluorescent radiation from the samples has been modeled. Growth of the mature scale and the distribution of elements therein have been determined within the constraints of the model. Diffusion of Fe and Ni atoms into the Cr_2O_3 scale was observed. Transient scale behavior was monitored in the evolving oxide scales. The major constituent of the developed scales was chromia. RXF depth profile data show that Fe diffuses into the Cr_2O_3 scale from the substrate and that diffusion is slower in the Y-containing alloy. Although RE elements produce improvement in the scale adhesion characteristics of Fe25Cr20Ni, all the samples show some susceptibility to spallation in the cycling oxidation experiment. RXF measurements acquired during isothermal oxidation were used to determine parabolic rate constants. Further modeling work is needed to quantify the effects of composition gradients and interface roughness on RXF.

ACKNOWLEDGEMENTS

The submitted manuscript has been created by the University of Chicago as Operator of Argonne National Laboratory ("Argonne") under Contract No. W-31-109-ENG-38 with the U. S. Department of Energy. The U. S. Government retains for itself, and others acting on its behalf, a paid-up, nonexclusive, irrevocable worldwide license in said article to reproduce, prepare derivative works, distribute copies to the public, and perform publicly and display publicly, by or on behalf of the Government.

REFERENCES

1. S. Haegawa, S. Ino, Y.Yamamoto, and H. Daineon, Jpn. J. Appl. Phys., **24**, L387, (1985).
2. Y. C. Sasaki and K. Hirokawa, Appl. Phys. Lett, **58**, 1384, (1991).
3. T. A. Robins, D. N. Ko, K. E. Gray et al., Appl. Phys. Lett., **66**, 2054, (1995).
4. H. P. Urbach and P. K. deBokx, Phys. Rev. **B53**, 3752, (1996).
5. R. S. Becker, J. A. Golovchenko and J. P. Patel, Phys. Rev. Lett., **50**, 153, (1983).
6. I. Koshelev, A. P. Paulikas and B. W. Veal, Oxidation of Metals (accepted).
7. T. A. Roberts and K. E. Gray, MRS Bulletin, **1**, 43, (1995).
8. A. Atkinson and R. I. Tailor, Transport in Non-Stoichiometric Compounds, Pergamon Press, New York, (1987).
9. A. Atkinson, Oxidation of Metals, **24**, 177, (1985).

Table I. Escape depths for fluorescent radiation emitted by the FeCr25Ni20 alloys and several oxides at two different take-off angles.

		Fe25Cr20Ni	Fe_3O_4	$FeCr_2O_4$	Fe_2O_3	NiO	$NiFe_2O_4$	Cr_2O_3
ρ (g/cm^3)		7.90	5.2	5.1	5.27	6.809	5.37	5.21
α_c	Cr Kβ	9.4		7.55				7.63
(mrad)	Fe Kα	8.7	7.06	7.0	7.094		7.18	
	Ni Kα	7.5				6.92	6.15	
$D(\alpha_c)$	Cr Kβ	160						260
(Å)	Fe Kα	107			250			
	Ni Kα	176				220		
D(90°)	Cr Kβ	15.6						42
(μ)	Fe Kα	7.48			40.7			
	Ni Kα	4.41				31.16		

Table II. Parameters found to fit the double layer model

700 °C	Overall Thickness (Å)	Ni containing Thickness (Å)	Ni concentration (%)	Fe containing Thickness (Å)	Fe concentration (%)
Fe25Cr20Ni	2400	1500	1.5	2000	30
Fe25Cr20Ni0.3Y	5000	3000	8	3500	30
Fe25Cr20Ni3Zr	2500	2300	1.5	600	15
800 °C					
Fe25Cr20Ni	12300	11200	2.5	11200	14
Fe25Cr20Ni0.3Y	9800	8800	4	7000	17
Fe25Cr20Ni3Zr	10200	10000	1	9400	19

Table III. Composition (EDX) of cross section of scales after the final (800 °C) oxidation.

Atomic species	Fe25Cr20Ni0.3Y	Fe25Cr20Ni3Zr	Fe25Cr20Ni
O, at%	70.11	66.78	63.79
Cr, at%	20.07	23.24	22.39
Fe, at%	7.45	7.83	10.82
Ni, at%	2.35	2.01	3.00
RE, at%	0.02<*	0.24	n/a

Table IV. Composition (EDX) of cross section of scales after isothermal 700 °C oxidation.

Atomic species	Fe25Cr20Ni0.3Y	Fe25Cr20Ni3Zr	Fe25Cr20Ni
O, at%	77.69	69.75	72.70
Cr, at%	19.49	27.50	25.60
Fe, at%	2.43	2.09	1.31
Ni, at%	0.42	0.64	0.38
RE, at%	n/a	n/a	n/a

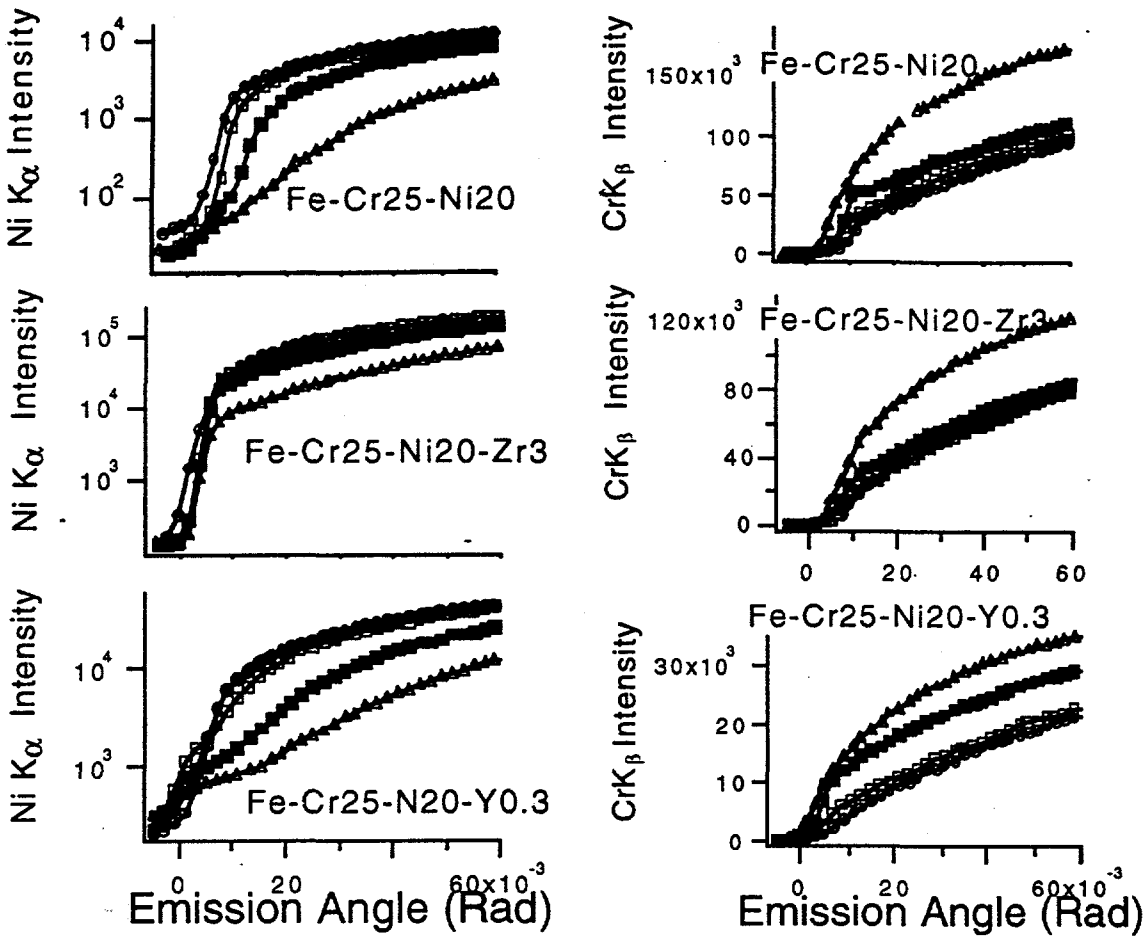

1. Ni $K\alpha$ and Cr $K\beta$ x-ray fluorescence intensity vs. emission angle after varying degrees of cyclic oxidation of the three alloys studied: circles--unoxidized; open squares--600 °C; full squares--700 °C; triangles--800 °C. Scale for Cr $I(\alpha)$ is linear; for the Ni, logarithmic.

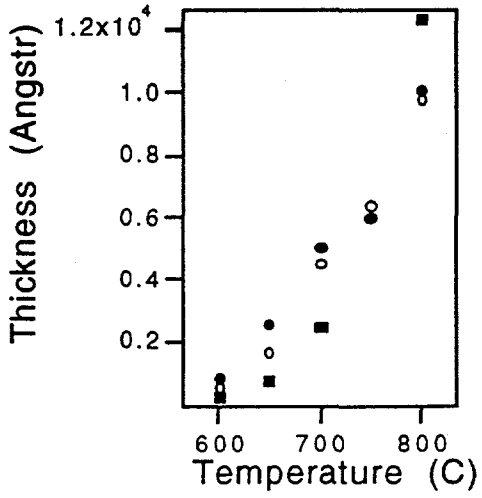

2. Thickness of scale formed during cyclic oxidation up to the temperature indicated. Open circles: Y-containing alloy. Full circles: Zr-containing alloy. Squares: base alloy.

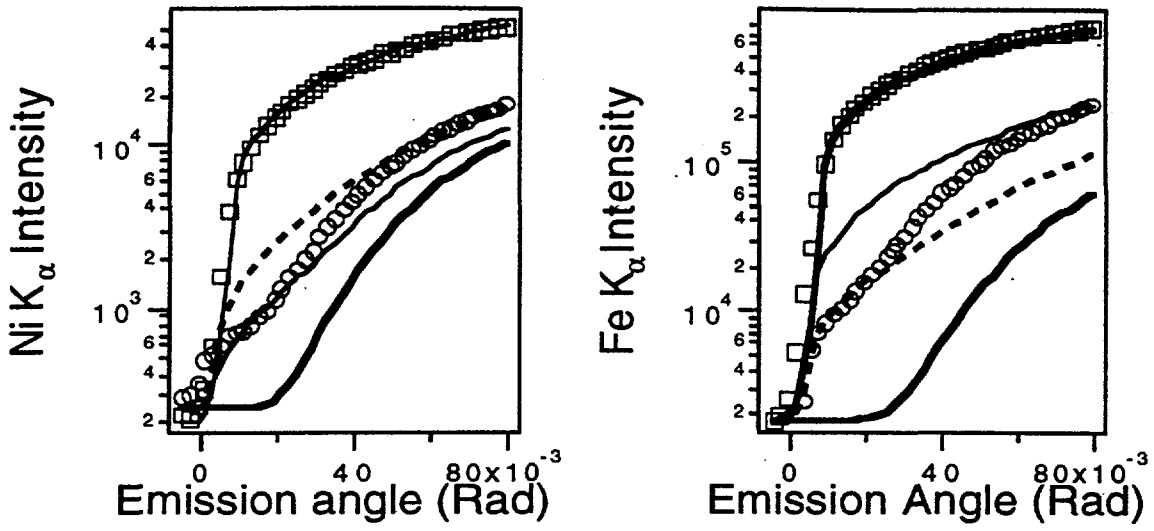

3. Examples of fits to the single-layer model. Squares and uppermost line: Data and fit to unoxidized specimen (bare metal). Lowest (heavy) line: expected $I(\alpha)$ for metal covered by a pure chromia scale 1 micron thick -- clearly not realistic. Circles: actual measured $I(\alpha)$ for the Zr-containing alloy (right) and the Y-containing alloy (left) oxidized at 800°C. The thin line on the left corresponds to the expected $I(\alpha)$ for a metal substrate covered by a 1 micron chromia scale containing 1% Ni, uniformly distributed throughout the scale; the dashed line on the left to the same configuration but with 2.5% Ni uniformly distributed throughout the scale. Similarly, on the right the dashed line corresponds to the expected $I(\alpha)$ for a metal substrate covered by a 1 micron chromia scale containing 6% Fe, uniformly distributed throughout the scale; the thin line on the right to the same configuration but with 17% Fe uniformly distributed throughout the scale

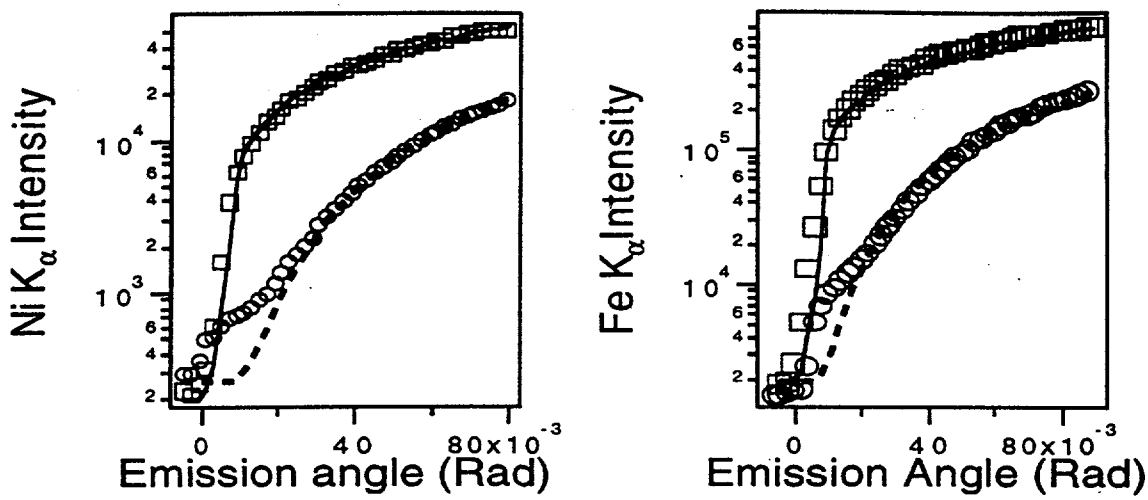

4. Examples of fits to the double-layer model (see text). Data are the same as in Fig. 3. Dashed line: in the left figure, a 0.1 micron layer of pure chromia is assumed to overlay a 0.9 micron layer of chromia which contains 4% Ni ; in the right figure, a 0.06micron layer of pure chromia is assumed to overlay a 0.94 micron layer of chromia which contains 19% Fe.

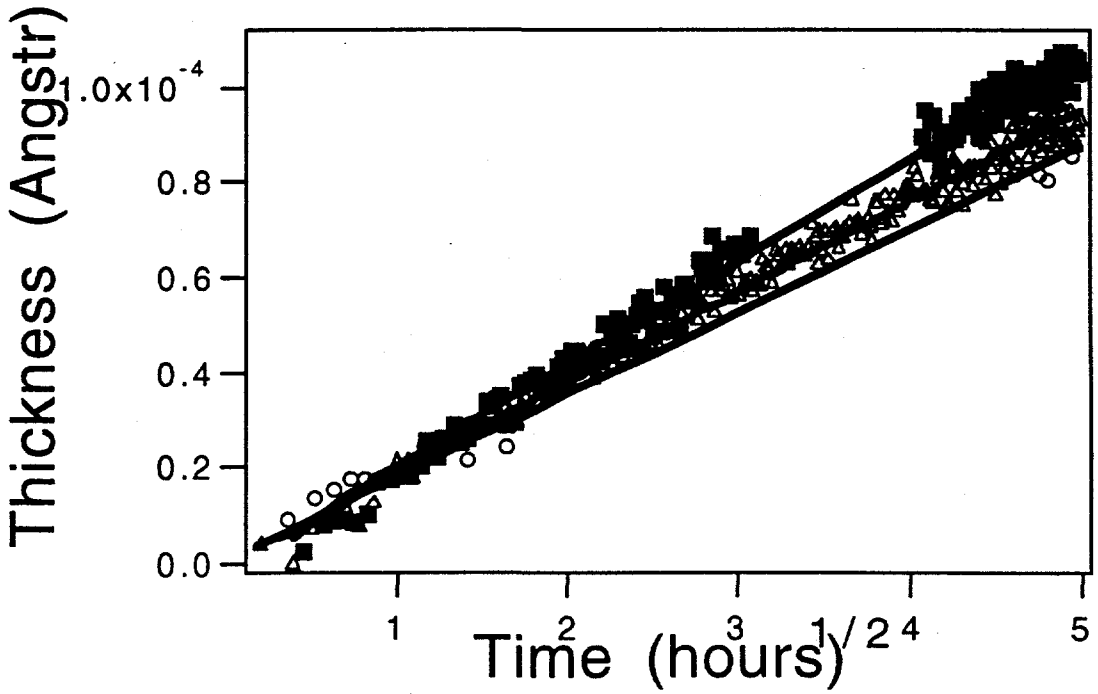

5. Isothermal oxidation at 700 °C in 13.3 Pa oxygen. Squares -- Fe25Cr20Ni (base alloy); triangles -- Fe25Cr20Ni3Zr; circles -- Fe25Cr20Ni0.3Y